Bentonite-Chitosan composites or beads for lead (Pb) adsorption: Design, preparation, and characterisation

MAJIYA, Hassan, CLEGG, Francis <http://orcid.org/0000-0002-9566-5739> and SAMMON, Chris <http://orcid.org/0000-0003-1714-1726>

Bentonite-Chitosan composites or beads for lead (Pb) adsorption: design, preparation, and characterisation

Hassan Majiya[1, 2*], Francis Clegg[1], Chris Sammon[1]

[1]*Materials and Engineering Research Institute, Sheffield Hallam University, City Campus, Sheffield, S1 1WB, South Yorkshire, UK*
[2] *Ibrahim Badamasi Babangida University, Lapai, Niger, Nigeria*

**Corresponding author*
E-mail address: majiyahassan@gmail.com (Hassan Majiya).

Abstract

This study investigated the efficiency of mixing bentonite with chitosan via different preparation methods, subsequently the different forms were investigated for their ability to remove Pb(II) ions from solution. The different forms of bentonite-chitosan (Bt-Ch), composites and beads, were prepared via solution blending and precipitation methods, respectively and in the weight ratios of 90%/10%, 70%/30% and 50%/50%. The beads were further subdivided, identified as "beads-A" and "beads-B", and were formed by adding either bentonite suspension or bentonite powder, respectively, to solubilised chitosan solution. The composites and beads were characterised by X-ray fluorescence (XRF), thermogravimetric analysis (TGA), X-ray diffraction (XRD), Fourier transform infrared spectroscopy (FTIR) and pH at zero point charge. XRF analysis showed a cation exchange mechanism occurred when chitosan was initially mixed with the bentonite. TGA results confirmed that beads contained more chitosan compared to their corresponding weight ratio equivalent composites. XRD results showed that chitosan was intercalated within the interlayer space of the bentonite for Bt-Ch composites and Bt-Ch beads-A and that the interlayer spacings increased with increasing chitosan loading. Though similar amounts of chitosan were present in both Bt-Ch beads-A and beads-B, there were fewer reflection shifts for beads B suggesting less intercalation of chitosan when the bentonite was added as a powder. FTIR spectra from the Bt-Ch composites and beads confirmed the presence of both chitosan and bentonite, and the N-H bands of chitosan shifted to lower frequencies demonstrating their involvement in the bonding mechanism of chitosan with bentonite. The experimental adsorption data correlated well with both non-linear Langmuir and Freundlich isotherm models, and in which both chemisorption and physisorption processes played crucial roles. The Langmuir-maximum adsorption capacities of Pb(II) ions for all the analysed

Bt-Ch composites and beads was found to range from 42.48 ± 4.22 to 94.60 ± 5.63 mg/g. The amount of chitosan present in the adsorbent and its distribution within or outside the interlayer space of the bentonite was shown to have pronounced effects on the Pb (II) uptake by the different Bt-Ch composites/beads, and although the chitosan greatly enhanced the adsorption of Pb(II) a cation exchange mechanism with the clay was still a dominant process. The adsorption of Pb(II) was also significantly affected by the presence of other multi-competing ions. Moreover, the developed Bt-Ch composites/beads exhibited good potential for re-use after five cycles of regeneration, thus, indicating their potential as cost-effective adsorbents for removal of Pb(II) ions from both drinking and wastewater.

Keywords: Bentonite-Chitosan composites / beads, solution blending, precipitation method, Pb adsorption isotherms.

1.0 Introduction

Water contamination by toxic metals is a global environmental burden as it affects the quality of drinking water and hence human health. Lead (Pb) is one of the most toxic metals of public concern and even at low concentration, it can cause extended destruction to numerous biological systems (Wang et al., 2014; He et al., 2015; Deng et al., 2019; Fei and Hu, 2022). Industrial effluents from manufacturing of lead-acid batteries and mining activities are the major source of Pb contamination in water and other environmental media (Nuhu and Hassan, 2014; Hassan et al., 2015; Liu et al., 2016). Of all the current methods researched in remediating metal-contaminated waters, adsorption is currently considered the most efficient and cost-benefit method, especially when cheap and sustainable materials are used as adsorbent (Babel and Agustiono Kurniawan, 2003; Crini, 2005; Yvonne Ligaya et al., 2013; Saad et al., 2013; Chen et al., 2014; Ren et al., 2014; Wang et al., 2014; He et al., 2015; Zhang et al., 2017; Yang et al., 2020; Fei and Hu, 2022; Taghavi et al., 2022). Although, scattered research has already been done on numerous alternatives and potentially lower-cost sorbent materials (such as zeolites, biochar, agro-waste, clay minerals

and polymers) for heavy metals uptake from contaminated water, more attention has recently shifted to combinations of clay minerals (e.g. bentonite, kaolinite) and biopolymers (e.g. chitosan or alginate) due to their excellent individual metal-binding capacities, availability, environmentally friendly nature and low-cost (Babel and Agustiono Kurniawan, 2003). Among the different clays, bentonite (mainly montmorillonite) is very abundant in nature, is widely used for metal sorption processes and as a raw material is good for composite formation in many applications (Gopal Bhattacharyya and Gupta, 2008; Kotal and Bhowmick, 2015). However, due to their relatively small size, a poor ability to quickly pass water through and the difficulty to recover all the clay particles from solutions after particular adsorption processes, neat clays are less attractive for treatment of water contaminated with heavy metals (Gopal Bhattacharyya and Gupta, 2008). To overcome these problems, clays are combined with other materials and modifications performed to date to improve their sorption capacity (and other properties) include the incorporation of other sorptive materials, such as chitosan (Liu et al., 2015), calcium alginate (Shang Tan et al., 2014) and activated carbon (Benhouria et al., 2015).

For decades, chitosan biopolymers have been used for many applications because of their unique chemistry and fantastic chelating properties (Guibal, 2004; Crini, 2005; Rinaudo, 2006; Pillai et al., 2009; Majiya et al., 2019). The presence of amine (-NH_2) and hydroxyl (-HO) functional groups in their polymer structure contributes to both polyelectrolyte and chelating properties (Guibal, 2004; Crini, 2005; Pillai et al., 2009). Chitosan is an abundant biopolymer and is derived from alkaline deacetylation of chitin, which is sourced majorly from waste of sea animals (i.e. the shell of crustaceans) obtained from food and fishery industries (Crini, 2005; Miretzky and Cirelli, 2009). Even though chitosan has been effective for metal ion adsorption, more modifications are still needed to improved its fragile nature before a workable implementation at the industrial scale is achievable (Miretzky and Cirelli, 2009). The combination of the biopolymer chitosan with clay has been reported to improve their chemical and mechanical stability, which in turn also enhances its adsorption capacity. Also, since it will be more expensive to use chitosan alone as an adsorbent in the remediation of wastewater (or drinking water) contaminated with heavy metals, the combination of chitosan with clay (such as bentonite) cannot only ensure sustainability but also have potential to offer a cost-benefit.

Only a limited number of studies have been published regarding the absorption of Pb (as well as other heavy metals) by bentonite-chitosan (Bt-Ch) composites (Futalan et al., 2010; Tirtom et al., 2012a; Hu et al., 2017). The heavy metals studied in order to assess the feasibility of using bentonite-chitosan composite materials includes, copper (II) (Futalan et al., 2010; Dalida et al., 2011; Cho et al., 2012; Pereira et al., 2013), lead (II) (Futalan et al., 2010; Tirtom et al., 2012a; Hu et al., 2017), nickel (II) (Futalan et al., 2010; Tirtom et al., 2012b), indium (III) (Jane-Calagui et al., 2014), arsenic (V) (Cho et al., 2012), palladium (II) (Liu et al., 2016), cobalt (II) (Wang et al., 2014), and cadmium (II) (Tirtom et al., 2012b).

The most popular method of preparing Bt-Ch composite materials is by a solution blending method, which involves mixing of solubilised chitosan (usually in dilute aqueous acetic acid) with aqueous bentonite suspension followed by centrifugation to remove water and non-adsorbed material (Darder et al., 2003, 2004; Alemdar et al., 2005; Ruiz-Hitzky et al., 2005; Lertsutthiwong et al., 2012; Giannakas, 2018). Darder et al. (2003), exclusively reported that the initial chitosan-clay ratio employed in their composite preparation did not necessarily reflect the final chitosan biopolymer amount adsorbed on the clay, which is likely to be due to loss of solubilised, unabsorbed chitosan during the washing step of the composite formation. Knowing the amount of the chitosan available (and position with respect to the clays interlayer) in the synthesised composites is critical to providing more understanding about their application, true composition, and form.

Herein, the amount of chitosan in the final clay-polymer composites are determined with respect to, starting and final compositions, location of chitosan within the clay and preparation procedure. A series of Bt-Ch composites and beads were developed. A solution blending method was used to produce mixtures termed ‘composites’, and a precipitation

method was used to produce mixtures termed 'beads'. The formation of precipitated beads has been investigated previously with both chitosan (Dalida et al., 2011; Tirtom et al., 2012a, 2012c; Jane-Calagui et al., 2014) and other similar materials such as alginate (Oladipo and Gazi, 2014, 2015), they offer a means to allow quick passage of water through a bed of adsorbent and minimal and economic preparation procedures. Both composites and beads were characterised by a range of different techniques including determining the pH of zero-point charge (pH_{zpc}), X-ray fluorescence, thermogravimetric analysis (TGA), X-ray diffraction (XRD), and Fourier transform infra-red (FTIR) spectroscopy. The prepared Bt-Ch composites and beads were applied (as adsorbents) within batch adsorption procedures to abstract Pb(II) ions from prepared aqueous solutions. Centrifuged supernatants after adsorption experiments were analysed for unabsorbed Pb (II) ions using inductively coupled plasma optical emission spectrometry (ICP-OES). A non-linear modelling method was employed to analyse the adsorption equilibrium process and optimisation was done using the "Solver add-in" in Excel Microsoft 365. Regeneration of adsorbents and selectivity towards Pb (II) adsorption in the presence of Cu, Zn, Ni and As was also assessed.

2.0 Experimental section

2.1 Materials and Methods

The bentonite, Cloisite® Na^+, was obtained from Rockwood Additives (now BYK Limited) and used as the layered silicate starting material. The bentonite was not sized fraction and was used as received to best represent material ultimately to be used in application, such processing in application would be an unnecessary expense. However, Cloisite Na+ when compared to others is considered a high purity bentonite with high montmorillonite composition (Breen et al., 2019). Chitosan biopolymer (190,000 – 310,000 medium

molecular weight; 75 – 85% deacetylated) was obtained from Merck. Acetic acid (≥ 99.99% - metal purity based), hydrochloric acid (32% w/v; specific gravity = 1.16) and nitric acid (69% w/v; specific gravity = 1.41) were used to prepared aqueous acidic solutions. Sodium hydroxide (reagent grade, 97%, pellets) was used to prepare aqueous basic solutions. Acetic acid, sodium hydroxide, lead (II) nitrate (≥ 99.95%), copper (II) nitrate hydrate (≥ 99.95%), zinc (II) nitrate (≥ 99.95%), nickel (II) nitrate (≥ 99.95%), sodium (meta) arsenite (≥ 90.0%), and the stock standard solutions (for ICP) of Pb(II), Cu(II), Zn(II), Ni(II), As(III), Ca(II) Mg(II), K(I) and Na(I) were also obtained from Merck, while hydrochloric acid and nitric acid were obtained from Fisher Scientific, UK. All chemicals used, unless otherwise stated, were of analytical grade purity and aqueous preparations were made using ultrapure deionised water.

2.2 Preparation of Bentonite-Chitosan (Bt-Ch) composites and beads

Two different preparation methods were investigated; i) solution blending to form composites, and ii) precipitation to form beads-A and beads-B.

2.2.1 Solution blending method

Chitosan solution was prepared by dissolving appropriate mass (see Table 1) of chitosan into a specific volume of 0.5% w/v aqueous acetic acid solution accompanied by vigorous stirring (650 rpm) for 2 hours using a magnetic stirrer. At the same time, bentonite was allowed to undergo a partial swelling in an appropriate volume (see Table 1) of deionised water and stirred (650 rpm) for 1 hour. Thereafter, the chitosan solution was slowly added to the bentonite suspension and the mixture stirred (650 rpm) for 24 hours at 60 °C. The resulting homogenised mixture was centrifuged at 3000 rpm for 2 hours using a Sorvall RC6 Superspeed centrifuge. The sediment (wet composite) was separated from the supernatant

and as part of a cleaning process approximately 300 ml of deionised water was added to the sediment, shaken (using a Stuart Rotator STR4 Mixer) for 2 hours and the mixture centrifuged again as above. This process was further repeated twice. Finally, drying of the sediment was carried out at a temperature of 70 °C overnight using a conventional oven.

2.2.2 Precipitation method

The Bt-Ch beads were prepared using a procedure reported in the literature (Wan et al., 2004) with modifications. First, chitosan solution was prepared by dissolving an appropriate mass of chitosan (Table 1) in aqueous HCl solution (0.25% w/v; 350 ml capacity) and stirring at 650 rpm for 2 hours. Then either 100 ml of bentonite suspension (as prepared above and for synthesis of beads-A) or appropriate weight of dry, powdered bentonite (for synthesis of beads-B) was slowly added to the chitosan solution and continuously stirred for another 24 hours at 650 rpm. A pH electrode was then placed into the beaker (containing Bt-Ch mixtures) and a burette was suitably positioned to allow addition of NaOH solution (1.0 M). The pH of the mixture was measured and recorded before any addition of NaOH solution. As the stirring of the mixture continued (450 rpm), NaOH solution from the burette was carefully added to the Bt-Ch mixture until its neutralisation (pH 7) and the polymer precipitated from solution. The precipitate (wet Bt-Ch beads) was separated from supernatant using a Fisherbrand test sieve (250 µm mesh) and washed three times with 200 ml of deionised water. It was then dried in an oven for 24 hours at 70 °C. The introduction of dry powdered bentonite was performed in order to induce a more disordered blend of chitosan and bentonite.

Photographs of the composites and beads, prior to drying, are presented in the Supplementary section (Figure S1) and show their different forms. When wet the

composites are a homogenous, weak paste whereas the beads are bead-like (spherical gels) in appearance, when dry they both resemble typical bentonite powders.

2.3 Percentage product yield of Bt-Ch composites and beads recovered

The percentage yield of Bt-Ch composite and beads produced via the solution and precipitation methods were calculated using Equation 1:

$$\text{Percentage (\%) yield} = \frac{\text{Actual yield}}{\text{Theoretical yield}} \times 100 \quad (1)$$

The actual yield represents the amount of product recovered from experiment after drying and the theoretical yield is the amount of product based on the sum of the starting materials.

2.4 Physicochemical properties and characterisation of Bt-Ch composites/beads

The Bt-Ch composites and beads samples were characterised by determining the pH of zero point charge and using XRF, TGA , XRD, and FTIR.

The pH of zero-point charge (pH_{zpc}) of the Bt-Ch composites/beads was determined using the pH-drift method as described in the literature (Lopez-Ramon et al., 1999; Zhang et al., 2016; Das et al., 2018) with modification. The detailed description of the procedure is presented in the Supplementary section (Table S1).

XRF measurements were performed using a Primus IV XRF spectrometer (Rigaku Model) equipped with an X-ray tube. All analyses were performed using quantitative methodology (H. L. Giles, P. W. Hurley, 1995) involving a fusion bead made from 0.2 g of sample and 10 g of lithium tetraborate/lithium iodide flux.

TGA of Bt-Ch samples was performed using a computer programmed TGA/DSC-1 instrument (Mettler-Toledo; Star^{e} System). All analyses were performed with 5 mg samples in alumina crucibles under an air purge (40 ml/min) and heated between 35 and 1000^{o}C using a heating rate 20 ^{o}C / min. The methodology used to determine the amounts of chitosan loaded onto the bentonites is described in detail in the Supplementary section (Table S2, Figure S2).

XRD analysis of Bt-Ch samples was performed using a computer programmed Philips X'Pert X-ray diffractometer (with pixel detector). A slit (1/16 degree) was mounted in front of the detector to reduce the number of channels. The XRD pattern was collected within a scan range from 2 - 45^{o} (2θ) using Cu target (λ = 0.1541 nm) radiation at supplied anode power 40 kV and 40 mA.

FTIR spectra were collected using a Nexus-Nicolet FTIR spectrometer coupled with an attenuated total reflection (ATR) accessory containing a diamond crystal. Spectra were recorded in the wavenumber range of 4000 - 500 cm^{-1} with a 4 cm^{-1} resolution and co-addition of 64 scans.

2.5 Batch adsorption experiments

The stock solution (1000 mg/L) of Pb(II) ions was prepared by dissolving 1.599 g of lead (II) nitrate in ultrapure deionised water and preserved with 10 ml of aqueous 5% w/v HNO_3 solution. The stock solutions of other ions (Cu(II), Zn(II), Ni(II) and As(III) for competing ions experiment) were also prepared by dissolving known weights of their salts in ultrapure deionised water and preserved by modifying with 10 ml of 5% HCl. Aqueous working solutions were prepared daily from the stock solutions by serial dilution.

Adsorption experiments were conducted in cleaned and sterilised Nalgene centrifuge plastic tubes (50 mL capacity). The centrifuge plastic bottles together with their contents were agitated using a Gyrotory Water Bath shaker (Model G76D; New Brunswick Scientific, Edison. N.J. U.S.A). After specified times, the mixtures were centrifuged (using a Sorvall RC6 Superspeed Centrifuge) at 3000 rpm for 5 minutes and the supernatant collected and stored in cleaned and sterilised Fisherbrand PP centrifuge tubes (15 mL capacity) that were appropriately labelled for analysis of Pb(II) ions. The quantitative measurement of Pb(II) ions was carried out by inductively coupled plasma – optical emission spectrometry (Agilent 5110 ICP-OES) using wavelength 220.353 nm, axial viewing mode and linear weighted calibration fit as measurement conditions. This procedure was followed when determining the adsorption equilibrium, adsorption efficiency and effect of competing ions (using multi-component solutions).

The effect of pH on the adsorption of the Pb(II) ion was carried out within a range not influenced by a precipitation process. Although a speciation experiment was not performed herein, Yang et al. (2010) has previously reported that about 99% of Pb(II) ions are in the free form when the solution pH is 2-5, while the predominant species of Pb(II) ions at pH > 7 are $Pb(OH)^{+}$, $Pb(OH)_2$, and $Pb(OH)_3^{-}$. Therefore, studying the effect of pH within the range of 7 and above could lead to erroneous conclusions. To ensure herein that Pb(II) ions are removed solely by adsorption processes and not by precipitation, the adsorption experiments were carried out at pH <7. In previous adsorption studies (Majiya, 2022), optimal Pb removal was achieved at a pH of 4.5 (between the range pH 2-6), and so was used throughout this adsorption study as the initial adjusted pH.

The following wavelengths 327.395, 206.200, 231.604, 278.022, 373.690, 279.078, 766.491, and 568.263 nm were selected during ICP-OES analysis of Cu(II), Zn(II), Ni(II), As(III), Ca(II), Mg(II), K(I) and Na(I), respectively.

The amount of Pb(II) ions per unit mass of Bt-Ch composites and beads (adsorbents), the percent adsorption performance (%) and the adsorption distribution coefficient (K_D; L/mg) were calculated using Equations 2, 3, and 4 respectively.

$$q_e = \frac{C_i - C_f}{M} \times V \quad (2)$$

$$\% \text{ Adsorption} = \frac{C_i - C_f}{C_i} \times 100 \quad (3)$$

$$K_D = \frac{q_e}{C_f} \quad (4)$$

Where q_e is the adsorption capacity (mg Pb(II) ions per gram Bt-Ch composites and beads), and C_i and C_f (mg L^{-1}) are the initial and final concentrations of the Pb(II) ions before and after the adsorption experiment, respectively. V (L) is the volume of solutions and M (g) is the mass of the Bt-Ch composites and beads (adsorbent).

2.5.1 Adsorption equilibrium study and isotherm modelling

An adsorption study was previously performed by surface response-optimal designs (manuscript in preparation) to examine how pH, initial concentration, and adsorbent dosage affect Pb adsorption. The results show that the adsorption capacity (mg/g) increases with pH and initial concentration, but decreases with adsorbent dosage, which is the most significant factor. The optimal experimental conditions (with respect to pH and adsorbent dosage) are used herein.

Accordingly, 0.05 g of each adsorbent (Bt-Ch composites/beads) was exposed to 25 mL of Pb (II) solutions with varying concentrations (10 - 500 mg L^{-1}) at pH 4.5. Pb(II) adsorption (onto Bt-Ch composites and beads) was very fast and reached equilibrium within 10 - 30 minutes thus a conservative agitation time of 60 minutes (with magnetic stirring speed of 230 rpm and at room temperature, approximately 21°C) was chosen for the equilibrium adsorption study. The equilibrium adsorption capacities, q_e (mg/g) were calculated and plotted against the corresponding respective equilibrium concentrations, Ce (mg/L) for adsorption isotherm modelling.

2.5.1.1 Langmuir isotherm model

The Langmuir isotherm model describes adsorption onto an adsorbate with homogenous surface and a fixed number of specific limited sites which have the same adsorption energies. It also correlates to a monolayer adsorption process and its non-linear equation can be expressed as in Equation 5 (Langmuir, 1916; Foo and Hameed, 2010; Tran et al., 2017);

$$q_e = \frac{Q_{max} k_L C_e}{1 + k_L C_e} \quad (5)$$

Where, q_e is the equilibrium adsorption capacity (mg/g), C_e is the equilibrium concentration (mg/L), Q_{max} is the maximum saturated monolayer adsorption capacity of an adsorbent (mg/g), and K_L is the Langmuir equilibrium constant (L/g). If the experimental data is adequately described by the Langmuir model, it is essential to calculate the separation factor (a dimensionless constant; R_L), because it reflects the favourability of adsorption and can be expressed as shown in Equation 6 (Hall et al., 1966; Webi and Ranjit K. Chakravort, 1974; Foo and Hameed, 2010; Tran et al., 2017).

$$R_L = \frac{1}{1+K_L C_o} \quad (6)$$

Where, K_L is the Langmuir equilibrium constant, and C_o (mg/L) is the initial adsorbate concentration. R_L values reflect the favourability of adsorption, adsorption nature is either unfavourable ($R_L > 1$), linear ($R_L = 1$), favourable ($0 < R_L < 1$) or irreversible ($R_L = 0$).

2.5.1.2 Freundlich isotherm model

The Freundlich isotherm is one of the earliest empirical equations used to describe equilibrium data and adsorption characteristics for a heterogeneous surface with possibility of multilayer adsorption. Since the surface will have different active sites, different adsorption energies are expected and the non-linear form of Freundlich equation can be expressed as shown in Equation 7 (Freundlich, 1906; Foo and Hameed, 2010; Tran et al., 2017);

$$q_e = k_f C_e^{\,n} \quad (7)$$

Where, K_F and n are the Freundlich isotherm constant (called the adsorbent capacity) and the adsorption intensity parameter (Freundlich exponent), respectively. The n value (dimensionless) ranges between 0 to 1 and is a measure of adsorption intensity. The n value close to zero indicates chemisorption, and a value close to unity signifies a physisorption process.

2.5.2 Desorption studies

The regeneration ability of the developed Bt-Ch composites and beads was carried out after exposing 0.2 g of each adsorbent to 150 mg/L Pb(II) solutions (25 ml; pH 4.5; agitation time = 10 minutes). After assessing the amounts of Pb adsorbed, the loaded adsorbents were agitated with 25 mL 1.0 M HCl for 120 minutes and filtered for recovered Pb(II) ions analysis. The treated adsorbents (with HCl to remove Pb) were stabilised with 10 ml of aqueous

NaOH (0.1 M) to return the pH to approximately pH 4.5 and then washed with 25 ml of de-ionised water (3 times) prior to re-use. The adsorption-desorption cycles were repeated 5 times to explore the reusability of Bt-Ch composites and beads. The percent desorption (%) was calculated using Equation 8 (Akpomie et al., 2015).

$$\% \text{ Desorption} = \frac{C_d V_d}{M q_e} \times 100 \quad (8)$$

Where C_d (mg/L) is the concentration of Pb (II) ions desorbed from Bt-Ch composites and beads, V_d (L) is the volume of desorbed solution, M (g) is the mass of adsorbent (Bt-Ch composites and beads), and q_e (mg/g) is the adsorption capacity of Bt-Ch composites and beads for Pb(II) ions.

2.5.3 Ion-Exchange experiments

Ion exchange experiments were carried out to help understand the adsorption mechanism, i.e. via cation exchange with the clay or with the chitosan, and were based on a procedure previously reported in the literature (Šćiban et al., 2006; Ngah and Fatinathan, 2009, 2010). The optimum experimental conditions described above were used with the range of 10 – 90 mg/L of Pb(II) ions solutions for all the adsorbent samples. The initial pH of the solution was adjusted to 4.5, and the final pH of the solution was also measured after the adsorption. The amounts of Pb(II) adsorbed and cations (Ca^{2+}, Mg^{2+}, K^{+} and Na^{+} ions) released were quantitatively determined by ICP-OES. To determine the possibility of leaching of these four cations from the adsorbents, a blank experiment was also conducted for the adsorbent with only deionised water. The net release of cations was calculated by subtracting the amounts of cations released from the blank experiments from the amounts of cations measured in the effluent after Pb(II) ions adsorption.

3.0 Results and Discussion

3.1 Synthesis and physicochemical properties of Bt-Ch composites and beads; yield, TGA and XRF analysis

The product yields for Bt-Ch composites, beads-A and beads B are shown in Figure 1A. When reduction in yield is observed it is generally due to loss of chitosan, but in some instances small amounts of bentonite were also observed to be washed away. The initial clay and chitosan mass includes adsorbed water (≈ 5-8 wt. % as evidenced by TGA), which is predominantly associated with the polarising exchangeable cations of bentonite or polar molecular groups of chitosan. When chitosan interacts with the bentonite the amounts of water can reduce (as evidenced by TGA) and is presumably due to direct interaction between the exchangeable cations and polar molecular groups resulting in fewer sites for the adsorption of water and hence less water overall. This water removal does contribute to a reduction in the yield, and also makes quantification more difficult.

Considering first the three composites prepared via the solution blending method, there is a decreasing yield with increasing chitosan offered. Supporting TGA data (Figure 1 – blue bars) and FTIR shows that significant chitosan is lost, but also suggests a fraction of bentonite is removed during the intensive washing procedures. Soluble components of the bentonite (NaCl and $NaSO_4$) will also be removed.

A comparison of the composites with the beads shows greater yields for the latter samples, which were prepared by the precipitation method. Although more chitosan was retained by the beads as evidenced by TGA, the decrease in their yields was also attributed to a loss of bentonite, this was particularly noticeable when powdered bentonite was added (beads B) since the washes collected during the washing stage were slightly cloudier showing the presence of some small amounts of bentonite. The yields of beads B were slightly lower, and

more so for 70/30 samples, than their respectively chitosan loaded beads A samples and this is despite similar amounts of chitosan being present as evidenced by TGA. It therefore suggests that both bentonite and chitosan are being lost during their preparation. The chitosan could be lost as an adsorbed species on the lost bentonite, but could also be lost as simply solubilised chitosan. Bentonite could also be lost directly if it was unable to be trapped by complexation with the chitosan.

Essentially, the TGA data emphasises that similar amounts of chitosan were adsorbed for beads A and B samples, and the although the amounts of chitosan retained increased with increasing chitosan offered, they were much less than those for the composites when treated with the higher amounts of chitosan.

The chemical compositions of Na-bentonite, Bt-Ch composites, and beads as measured by XRF are shown in Table S3 of the Supplementary section. Of particular note are the amounts of Na as these can be related to the cation exchange capacity (CEC) of the bentonite, the amounts of Na removed during the mixing with chitosan and the amounts of Na residing after the chitosan precipitation (using NaOH) and subsequent washing process used for beads A and B.

Washing the bentonite removes the extraneous Na present as NaCl and $NaSO_4$ revealing the amounts (2.80 mass %) relative to the CEC (92.5 meq/100 g). When forming the 90-10, 70-30 and 50-50% Bt-Ch composites this amount reduces by 55, 51 and 64%, respectively showing that a cation exchange mechanism has occurred – this will be via the NH_4^+ ions of the chitosan with the Na^+ ions of the bentonite. The values could be considered similar for the 90-10 and 70-30 samples given the nature and reproducibility of the samples, but the higher exchange for the 50-50 Bt-Ch sample could be linked to the higher amounts of chitosan used. Any correlation from the amounts of Na in the beads A and B samples with

cation exchange processes is not possible but does show the extent of Na^+ remaining after the precipitation and washing process. It could be assumed that the extent of cation exchange in the beads A samples is very similar to that of the composites since they have experienced exactly the same preparation procedure prior to precipitation, at this stage the chitosan adsorption process will be more or less complete and further exchange will be limited due to very limited chitosan molecular chain movement once adsorbed. Desorption and then re-adsorption is highly unlikely since it would need all adsorption sites to be removed simultaneously for sufficient molecular movement and the probability is very high. Beads B samples could have experienced less cation exchange since there is less chitosan within the interlayer space as evidenced by XRD (discussed below).

3.2 pH of zero-point charge

The pH_{zpc} for the composites (5.8), beads A (6.6 – 7.0) and beads B (6.6 – 7.0) were lower than both the pristine bentonite (9.8) and chitosan (8.0) (curves shown in Figure S3 in Supplementary section). Combining the chitosan and bentonite therefore greatly changed their overall surface and this results from the strong interaction between the two and at specific adsorption sites (the cation exchange sites and broken edge sites of the bentonite and polar groups of chitosan, NH_4^+). Below the pH_{zpc} values the surface is positively charged and above negatively charged [33], the adsorption experiments performed herein were conducted at pH 4.5 and so the adsorbents were positively charged prior to the addition of the adsorbates (heavy metals).

Specific surface area measurements by the BET nitrogen adsorption method have unable to be collected for samples herein. Literature values (Lima Patrício et al., 2012) for Cloisite Na^+ are reported as 32 m^2/g, which is typical of other Na-bentonites with relatively high CEC (Moussout et al., 2018), but can range between 10 – 130 m^2/g. Futalan et al. (2010),

modified bentonite with BET surface area of 84.28 m^2/g and when complexing with approximately 5 wt. % chitosan this reduced to 33.17 m^2/g. It is therefore anticipated lower values would be observed for the composites and beads herein. It is important to consider that specific surface area measurements are conducted on dried particles, whereas adsorption experiments are conducted in aqueous medium, thus their form considerable changes in the swollen state and it is therefore not a straightforward correlation between surface area, pore type, pore volume and adsorption capacity.

Interestingly the aqueous swelling volumes of the composites and beads A do vary and also with respect to chitosan loadings (Figure S4 in Supplementary section). Note the swelling experiments are performed on composites and beads that have been dried first and then re-dispersed in water (as in the adsorption experiments) and that the beads do not reform upon rehydration. Swelling volumes reduce compared to bentonite alone (100%) and are similar when the amounts of chitosan are the same (all composites and 90%Bt-10%Ch beads A). When more chitosan is present, as for example with 70%Bt-30%Ch beads A, the swelling volume does increase. However, this is not always the case as with 50%Bt-50%Ch beads A (43 wt% compared to 26 wt% for 70%Bt-30%Ch beads A) a lower swelling volume occurs. Differences could be due to variances in Na^+ salt solution concentration as there is a correlation with Na^+ amounts determined by XRF (Table S3), but other factors will contribute, such as surface charges. Although there are no correlations with Pb adsorption levels, the main point to realise is that the composites and beads do swell considerably when re-dispersed in water.

3.3 XRD Analysis

XRD was used to determine whether the chitosan was located within the interlayer of the bentonite clay. The XRD patterns of all prepared composites and beads are shown in Figure 2. The XRD pattern for chitosan (see Supplementary section - Figure S5) shows two main reflections at about 10 and 20 °2θ, these are not present in any of the Bt-Ch samples and shows that the crystalline nature has been completely disrupted. There is no contribution from crystalline chitosan to the interpretation of the bentonite reflections. The XRD A large increase in d-spacing from 1.26 nm to 1.59, 1.72 or 1.75 nm was observed for 90%Bt-10%Ch, 70%Bt-30%Ch and 50%Bt-50%Ch composites, respectively. For Bt-Ch beads-A, and like for the composites, the d-spacing reflections show a shift towards lower angle (larger d-spacing) and a large difference compared to pristine clay. However, there are differences in relative intensities of the reflections and thus interlayer spacings and chitosan distribution between the beads A and composite samples. This is anticipated given the higher loadings of chitosan in beads A as determined by the TGA analysis (Figure 1B). The calculated d-spacings of 1.87, 1.92 and 2.02 nm were observed for 90%Bt-10%Ch, 70%Bt-30%Ch and 50%Bt-50%Ch beads-A, respectively. Shoulders towards higher angles of these reflections and at slightly higher angles than bentonite are still clearly observed for both 90%Bt-10%Ch, 70%Bt-30%Ch beads-A and these represent single layers of chitosan between the clay layers. The relative amounts of these single layers decrease with increasing amounts of chitosan, as expected since the additional chitosan will convert single layers into bilayers. The higher d-spacing value obtained with the highest amount of chitosan (50%Bt-50%Ch beads-A) indicates that there are predominantly bilayers of chitosan intercalated between the clay layers. This agrees with the similar higher d_{001}-spacing value (2.04 nm) obtained from the previous work carried out by Darder et al. (Darder et al., 2003, 2004), which has been related to chitosan bilayers intercalated into clay structures. For the XRD traces collected

from all Bt-Ch beads-B samples, the dominant reflections were positioned at 1.26 nm indicating higher proportions of single layer loadings, which is in strong contrast to the observations noted for the composite and beads A samples. There is some evidence of bilayers structures in the Bt-Ch beads-B samples, as evidenced by the shoulders representing d_{001}-spacings of approximately 1.75 nm, but their intensities and thus inferred amounts are significantly less. Similar reflection shifts may have been expected for beads-B in comparison to beads-A because similar amounts of chitosan are present (Figure 1B), however this was not the case. The shifts are even lower than those of the composites, which have considerably less chitosan present. Thus, this data suggests that the preparation process, i.e. the addition of dry, powdered bentonite rather than as an aqueous suspension greatly affects (i.e. lowers) the distribution of chitosan within the interlayer space of the clay (as illustrated in Figure 3). It is believed that before the bentonite is able to swell while immersed in water, the solubilised chitosan molecules strongly adsorb onto the surfaces and edges of stacked clay layers prohibiting them from separating and blocking chitosan from entering between the layers.

3.4 FTIR Analysis

Fourier transform infrared spectroscopy was used to assess chemical interactions between the chitosan and bentonite. Figure 4 shows the FTIR spectra of bentonite, Bt-Ch beads-A, and chitosan. FTIR spectra of Bt-Ch beads-B and Bt-Ch composites samples are presented in the supplementary section (Figure S6 and S7, respectively).

The FTIR spectrum of pristine bentonite (Fig. 4a) shows dominant bands due to montmorillonite as reported in the literature (Pandey and Mishra, 2011); the band at 3627 cm^{-1} is attributed to the O-H stretching vibration of structural OH groups and the band at

1635 cm^{-1} is attributed to the O-H deformation vibration of adsorbed water molecules. The intense band at 1003 cm^{-1} corresponds to the Si-O stretching vibration bonds of montmorillonite.

The spectrum of pure chitosan (Fig. 4e) looks similar to that previously reported in the literature (Kadir et al., 2011; Nesic et al., 2012; J. Liu et al., 2016; Chen et al., 2018); the broad bands centred around 3282 cm^{-1} are due to overlapping bands from O-H and N-H stretching vibrations. The bands at 1648 cm^{-1} and 1564 cm^{-1} are due to C=O stretching vibration of the carboxamide group (O=C-NHR) and N-H bending vibration of amine groups ($-NH_2$), respectively. The bands at 1420 cm^{-1} and 1314 cm^{-1} are related to the bending vibration of -C-H bonds and the band at 1004 cm^{-1} is attributed to stretching vibrations of C-O groups.

The spectra of the Bt-Ch beads-A with different weight-ratios of chitosan (90%Bt-10%Ch, 70%Bt-30%Ch, and 50%Bt-50%Ch; Fig. 4b, 4c and 4d, respectively) are combinations of the spectra of bentonite and chitosan. The characteristic bentonite bands at 3627 cm^{-1} and 1008-1014 cm^{-1} appear in the spectra of all the Bt-Ch beads-A and the intensity of the former decreases with increasing chitosan loading. The chitosan bands between 1200-1600 cm^{1} also increase with chitosan loading and corresponds with the chitosan loadings derived by TGA. The band at 1648 cm^{-1} in pristine chitosan shifts to slightly lower frequencies for all the bead-A samples, however, it is not certain whether these band changes are due to a shift of the C=O stretching band of carboxamide or an overlap of the O-H deformation vibration of water molecules (as noted at 1635 cm^{-1} for bentonite). The N-H deformation band due to amine groups at 1564 cm^{-1} in the pristine chitosan does shift to lower frequencies for all Bt-Ch beads-A samples. A shift to lower frequencies would indicate a

lower degree of interaction of the N-H bond (i.e. less energy required to move the constrained hydrogen) when complexed with clay and presumably results from the breakup of a strong hydrogen-bonding network within the chitosan molecules when present alone, and a weaker N-H interaction with the clay. Since it was shown by XRD that there is less intercalated chitosan in bead B than bead A samples, (but relatively similar amounts of chitosan) different interactions of the N-H bonds may be occurring, however, there was no spectral evidence to suggest this as the spectra of the bead B samples similar (see supplementary data). It could be that the chitosan molecules interact with the clay more so via the carbonyl groups of the carboxamide group leaving the N-H bonds available to interact with Pb cations. This is not too unexpected since amide bands have been shown to preferentially interact via carbonyl groups (Breen et al., 2000).

The trends in the spectra of Bt-Ch composites samples were similar to those of bead A and B samples though the intensity of the bands due to chitosan were less intense, which was due to less chitosan being present. The presence of a very weak band at ≈1720 cm^{-1} was additionally observed for all the Bt-Ch composites and this was attributed to the ν_{CO} stretching band of traces of acetate ions present in the composites, that were introduced by the use of acetic acid to adjust pH (Darder et al., 2003).

3.5 Adsorption equilibrium and isotherms modelling

Adsorption isotherms were obtained by fitting experimental data to both Langmuir and Freundlich equations. Figure 5 illustrates both Langmuir and Freundlich isotherm models for Pb(II) adsorption by 90%Bt-10%Ch composites. The isotherm plots for the other adsorbent samples are presented in the Supplementary section (Figure S8), but values (or constants) obtained from Langmuir and Freundlich isotherm modelling for all the adsorbent samples

are presented in Table 2. Non-linear chi-square (X^2) was employed to assess the quality of the fits concerning the isotherm modelling of the adsorption of Pb(II) ions onto Bt-Ch composites and beads. Very low values (e.g., close to zero) indicate that experimental data is very close to data obtained using a model, and vice versa (Tran et al., 2017). The X^2 values yielded by both Langmuir and Freundlich models were small and fairly similar (Table 2), which is a positive result, but difficult to determine which of these models more precisely fit the data. On the other hand, the high correlation coefficient values of R^2 = 0.999 from the modelled data indicate that the equilibrium data obtained from Pb adsorption is consistent with Langmuir and Freundlich isotherms. It can therefore be stated that the adsorption of Pb onto Bt-Ch composites and beads is a monolayer process, which befits the expectations of the Langmuir model; however, the good fit to the Freundlich isotherm model also suggests that there is a range of active sites with a range of adsorption energies. The presence of both clay and chitosan in the composites and beads was responsible for the heterogeneous nature of the adsorbent, made up of multiple functional groups and active sites for Pb adsorption. This is similar to a previous study conducted by Ngah and Fatinathan (Ngah and Fatinathan, 2010), they observed that the equilibrium data obtained for Pb(II) biosorption (onto chitosan and chitosan-glutaraldehyde) fitted well for both Langmuir and Freundlich isotherm models.

The separation constant values, R_L, were calculated using Equation 4 and are given in Table 2. The R_L values were all found within the range of 0 to 1 indicating that the adsorption of Pb(II) ions onto all the adsorbents was favourable.

The Q_{max} value which represents the maximum adsorption capacity of Pb(II) ions at monolayer coverage as determined through the Langmuir isotherm, was much higher for Bt-

Ch beads compared to their corresponding, weight ratio treated, composites (Table 2). This correlates well with more chitosan present in the beads (as evidenced from TGA, Figure 1), and therefore, suggests more active sites through the chitosan are available for Pb (II) adsorption. Similar Q_{max} values may be anticipated for both beads-A and beads-B because of their similar amounts of chitosan present, however this is not the case. The Q_{max} values obtained for beads-A are lower than those of the corresponding beads-B, which suggests the distribution of chitosan within the interlayer space rather than on external surfaces of the bentonite clay (as evidenced by XRD results; Figure 2) can reduce Pb (II) uptake. The more active sites for Pb (II) adsorption in beads B could therefore be linked with more chitosan on external surfaces and/or more exchangeable sites within the clay interlayer. It is also noted that Q_{max} increases for beads-B with chitosan loading but not for beads-A (or composites), which suggests for beads B (and assuming the number of cation exchange sites in the clay remain constant) the higher amounts of chitosan outside the interlayer play a stronger role in contributing to more Pb adsorption.

To assess the respective contribution of either bentonite or chitosan towards Pb-adsorption in the composites and beads, the expected Q_{max} due to the fraction of chitosan in the composites or beads were estimated from the Q_{max} of 100% chitosan, which was found to be 116.97 ± 2.14 mg/g (see Supplementary section; Figure S9). The general observation is that the amounts of Pb adsorbed by the composites and beads is considerably more than that anticipated from the fraction of chitosan alone in the composites and beads (see Supplementary section; Figure S10), therefore it suggests either the bentonite clay also contributes towards Pb(II) adsorption or there is a synergistic adsorption mechanism between bentonite and chitosan enhancing Pb(II) adsorption. The contribution of a cation

exchange mechanism with the resident cations on the bentonite is discussed further below (Section 3.9).

The Q_{max} values obtained from adsorption of Pb(II) with Bt-Ch composites and beads were compared with other adsorbents reported in the literature (Table 3), and the higher adsorption capacities indicates that Bt-Ch composites and beads could serve as potential and better adsorbent. Futalan et al. (2010) studied the removal of Pb(II) ions from a single-component solution using chitosan-immobilized-on-bentonite and found an inferior Q_{max} value (26.39 mg/g), whilst using a similar optimum pH range as obtained in this study. However, they reported that the adsorbent used was prepared in the weight ratio of 95% bentonite clay and 5% chitosan biopolymer, which may account for lower Pb(II) uptake (mg/g) because less chitosan is present in the composite. Moreover, their procedure was more time-consuming, as it took about 4 hours to attain removal equilibrium at higher concentrations of Pb(II) ions. In this study, the adsorption of Pb(II) ions onto Bt-Ch composites/beads was very fast and reached equilibrium within 10 - 60 minutes. In another study, Tirtom et al. (2012a), reported the removal of Pb(II) ions using crosslinked chitosan-clay composite beads with maximum removal capacity (Q_{max}) of 7.93 mg/g, which is much smaller compared to the results obtained in this study. It was stated that the adsorbent was prepared by blending 50% bentonite clay and 50% chitosan in weight ratio, before being crosslinked using a solution containing glutaraldehyde. Despite its limited loading capability, the use of chitosan-clay composites as an adsorbent for the removal of metal ions could be relatively expensive due to the additional cross-linking process. Hu et al., (2017) demonstrated the removal of Pb(II) ions from a single-component solution using montmorillonite-chitosan composite, where the Q_{max} value was found to be 47.95 mg/g, but

it took more than 3 hours to attain equilibrium. The composition of this adsorbent was not explicitly quantified, yet it appears that it consists of 91% montmorillonite and 9% chitosan biopolymer with respect to weight proportion. Overall, Bt-Ch composites or beads represent a good alternative adsorbent for Pb(II) removal, considering its high loading capacity, fast adsorption equilibrium, and easy preparation of the composites and beads. Our study though does show that the preparation procedure and subsequent form needs to be carefully considered to optimise adsorption.

The estimated adsorbent capacities (also referred to as Freundlich constant, K_F) determined from the Freundlich isotherms, are generally high for all the Bt-Ch composites and beads concerning Pb(II) adsorption. The Freundlich constant (K_F) characterises the strength of the adsorption, and a higher K_F value indicates that higher loading of adsorbate (such as Pb(II) ions) onto adsorbent could be achieved (Worch, 2012). The observed Freundlich exponent (n) values calculated fall within the range of 0 to 1, and since it is closer to zero, this implies that the surfaces of these adsorbents in contact with Pb(II) ions are heterogeneous, a value below unity also usually suggests a chemisorption process (Foo and Hameed, 2010; Kang et al., 2013).

3.6 Adsorption efficiency of Pb(II) ions

To investigate the efficiency of the absorption process 0.2 g of bentonite, chitosan or Bt-Ch composites and beads were exposed to Pb(II) solutions (100 mg/L; pH of 4.5). After 60 minutes of agitation, almost complete removal of Pb(II) ions was observed for all Bt-Ch composites and beads (see Supplementary section; Figure S11). These results are comparable to that of pure chitosan and about 50% more when compared to pristine Na-bentonite (Figure S11). The excellent removal percentages (%) of Pb(II) by chitosan in

comparison to the pristine clay is presumably due to more adsorption sites. Although the bentonite alone performs less effectively, the 90%Bt-10%Ch composites and beads, which contain only a small proportion of chitosan (~10 wt.%) do almost completely remove all Pb ions. It would be interesting to compare the relative proportions of chitosan and bentonite in these composites and beads as single components to help determine whether a synergist adsorption process is being observed. Moreover, these high adsorption efficiencies support the potential use of Bt-Ch composites and beads as cost-effective adsorbents for removal of Pb(II) ions from both drinking and wastewater to the barest minimum safe levels.

3.7 Effect of competing ions

To investigate the selectivity of Bt-Ch composites and beads towards Pb(II) ions, batch adsorption experiments were conducted in the presence of other competing ions using multi-component metal solutions containing Pb(II), Zn(II), Cu(II), Ni(II) and As(III) ions, each with initial concentration of 100 mg/L. The removal percentages (%) of these metal ions from the multi-component solution are shown in Figure 6 and in general they show similar ratios across the different metal ions. One can see that the adsorption of Pb(II) from the multi-component solution by Bt-Ch composites and beads was significantly affected by the presence of other competing ions, and the calculated removal efficiencies showed lower values compared to those from a single component Pb(II) solution (Figure S11). This is because of different cation selectivities and the available adsorption sites on these adsorbents cannot accommodate all the metal ions at the same time. Relative to other competing ions, Pb experienced the highest removal percentages for 90%Bt-10%Ch, 70%Bt-30%Ch and 50%Bt-50%Ch composites and 90%Bt-10%Ch beads-A & beads-B, demonstrating their high affinity towards Pb. The common observation from these adsorbents is that they

contain less chitosan in their composition as evidenced by TGA (Figure 1B) and so indicating bentonite plays a stronger role over chitosan in Pb adsorption. The % removal extents followed the order Pb(II)>Cu(II)>Ni(II)>Zn(II)>As(III) for these adsorbents and correlated well with their electronegativities (1.9, 1.9, 1.8, 1.6 and 2, Pauling scale) with the exception for As. The exception for As is because of its negative charge and so behaves very different to the others. Excluding the consideration of As, the % removal extents order did not correlate with their respective ionic radii (77.5, 73, 69 and 74 Å) or their respective hydrated ion radii (4.01, 4.3, 4.04 and 4.3 Å). The deviation in correlation within the hydrated ion radii was only observed for Cu and this was also noted with the nitrate salt solubilities (59.7, 156, 94.2, 184.3 g/100 ml, 20°C, respectively). Solubility is a strong driving force for adsorption via a cation exchange mechanism on to clays and so this links well with the high Pb % removal percentages. The exception observed for Cu is linked to its preferential attraction to chitosan which is why Cu ions experienced their highest removal percentages with the adsorbents; 70%Bt-30%Ch and 50%Bt-50%Ch beads-A & beads-B, which contain more chitosan. It has been reported that among all the transition metals, Cu forms the most stable complexes with glucosamine (a monomer of chitosan biopolymer), and this correlates with the higher adsorption efficiency of Cu(II) ions by Bt-Ch beads (Muzzarelli, 1977). Also, a binary adsorption study carried out by Ngah and Fatinathan (2010), showed that chitosan-triphosphate beads had higher affinity for Cu(II) ions in comparison to Pb(II) ions (Ngah and Fatinathan, 2009). They reported that Cu(II) ions seem to be a stronger competitor, and its presence significantly depressed the adsorption of Pb(II) ions (Ngah and Fatinathan, 2009).

The adsorption distribution coefficients (K_d) of each metal ion investigated when compared across respective adsorbents (Table S4 in Supplementary data) show similar trends to

their % removal efficiencies (Figure 6). The highest K_d values represent the metal most likely to be adsorbed and were observed for Pb(II) in the majority of cases (i.e., 90%Bt-10%Ch, 70%Bt-30%Ch, and 50%Bt-50%Ch composites and 90%Bt-10%Ch beads-A & beads-B), these correlated well with the adsorbents having least amounts of chitosan. When higher amounts of chitosan were present (i.e., 70%Bt-30%Ch and 50%Bt-50%Ch beads-A & beads-B) very high K_d values were observed for the Cu ions whilst the Pb ions were ranked second highest. The lowest K_d values represent the metals most likely to remain in solution and for every adsorbent this was found to be As.

Overall, the fact that these adsorbents could remove a wide range of metal ions gives credence to their use as adsorbents for heavy metal remediation from water. Even though As adsorption is very minimal with these adsorbents and is related to its negative charge, a means to effectively enhance its adsorption has been achieved and is to be discussed in a separate publication.

3.8 Desorption studies and characterisation of regenerated Bt-Ch composites and beads

An appropriate adsorbent must not only be effective and have good adsorption capacity it should also allow for subsequent easy removal of metal ions (Ren et al., 2014; Akpomie et al., 2015; Vakili et al., 2019; Fei and Hu, 2022). Therefore, the desorption (recovery) of adsorbed Pb(II) ions and regeneration of Bt-Ch composites and beads were investigated. In this study, aqueous HCl solution was used as the stripping (desorbing) agent. The optimal recovery of Pb(II) ions was achieved with a 1.0 M concentration of aqueous HCl solution. HCl is an inorganic and strong acid widely used as cation-exchange agent for bentonite, in the desorption of metal ions from chitosan, its derivatives, and other adsorbents (Vakili et al.,

2019). The desorption process is achieved by supplying excess H^+ ions, which shifts the adsorption equilibrium in the favour of H+ adsorption, it effectively reduces the number of interactions between adsorption groups (such as -NH_2) and metal ions (e.g., Pb). At the same time, the chloride ions (from HCl) readily complex with metal ions and help to solubilise. Also, the concentration used was chosen because chitosan is highly unlikely to be soluble in 1.0 M HCl solutions, as was demonstrated in preliminary dissolution experiments (data not shown).

The Pb(II) adsorption and desorption percentages from 70%Bt-30%Ch composites and beads are shown in Figure 7. The respective plots for the other Bt-Ch composites and beads samples are presented in the Supplementary section (Figure S12). The desorption percentages in the 1st cycle observed for all the adsorbents was above 80%. This value, though slightly lower compared to adsorption percentages (about 90 to 99%), still portrayed good recoveries. For practical applications, it is imperative to investigate the stability of the same adsorbent by re-using it in multiple regeneration processes (adsorption-desorption cycles) (Akpomie et al., 2015; Vakili et al., 2019). In this regard, serial adsorption-desorption steps were conducted up to five times, and the observed percentages obtained for both adsorption and desorption of Pb(II) ions remained similar. This indicates that all the adsorbents were stable without apparent loss of the adsorption capacity for up to at least 5 cycles. Even though roughly 10-20% of Pb stayed attached to Bt-Ch composites/beads after each desorption operation, the successive adsorption process was highly proficient and remained consistent. The moderate consistency of the removal efficiency (%) observed for all adsorbents is attributed to the reversible active sites (such as the amino groups of chitosan and the cation exchange sites of bentonite) available for each successive

adsorption. The recyclable nature implies that, chitosan is still present in the regenerated Bt-Ch composites and beads, which is evidenced by TGA as shown in Figure 1. However, in comparison with initial chitosan loading (i.e. amount of chitosan before adsorption; Figure 1) some chitosan has been lost from 70%Bt-30%Ch beads-B (8.79 %), 50%Bt-50%Ch beads-A (25.4 %) and 50%Bt-50%Ch beads-B (12.88 %). This loss of chitosan demonstrates a potential reduction in the longevity of these particular, highly loaded chitosan adsorbents. It was noted that for the composites, but significantly for 70%Bt-30%Ch and 50%Bt-50%Ch, an unexpected higher amount of chitosan was present after desorption. This is possibly due to batch variability in the preparation of the Bt-Ch composites, but could also be due to protons (H^+) replacing Na^+ within the composites, a portion of the bentonite preferentially being lost during the repeated adsorption and desorption processes or even HCl solubilising a particular component of the bentonite. Overall, the results indicated that the Bt-Ch composites and beads exhibited good reusability and can be recovered for consecutive uses.

3.9 Adsorption mechanism

To help further understand the adsorption mechanism of Pb(II) ions on Bt-Ch composites and beads, for example, whether a cation exchange mechanism with the clay or interaction with chitosan occurs, changes in the pH of the Pb(II) solution were initially investigated and measured before and after the adsorption process. This is because H^+ ions can reside on clay; can protonate chitosan and the adsorbents have experienced acidic environments during preparation. It was observed that the pH of the solution increased after the adsorption of Pb(II) ions for all the adsorbents (from the adjusted pH of 4.5 ± 0.2 to 5.8 ± 0.9). A similar observation was also obtained by Ngah and Fatinathan (2010), when they studied the sorption of Pb(II) ions onto chitosan (and its derivatives). This could indicate that

H^+ ions in solution during the preparation become adsorbed onto the clay (in exchangeable cation sites or at broken edges) or protonate more N-H groups on the chitosan. From the control experiments (containing only adsorbents and no Pb) pH's of 6.5 ± 0.2 and 7.4 ± 0.2 were observed for Bt-Ch composites and beads, respectively and so increased pH changes after Pb(II) adsorption could simply be a balance between the pH's of the solution and that produced by the adsorbents. There is also the possibility that the protons (H^+) could be involved in a co-adsorption mechanism with the Pb(II) ions and other anions. In summary, if protons were present on the clay in cation exchange sites or associated with chitosan and were exchanged with Pb(II) ions then any correlations with adsorbent type and pH changes were not apparent to confirm the mechanistic role of H^+. Moreover, the pH changes equate to very minimal amounts of increases in H^+ ions desorbed (<1.5% of the CEC of clay component and <1.5% of available NH_2 groups on chitosan) relative to the amounts of Pb(II) ions adsorbed (~2-43% of the CEC) and so can be considered negligible or a small contributing factor to adsorption mechanisms. Of interest is that the pH changes (from the adjusted pH of 4.5 ± 0.2 to 5.8 ± 0.9) were below the pH_{pzc} of the adsorbents (composites (5.8), beads A (6.6 – 7.0) and beads B (6.6 – 7.0)) thus showing the adsorbents remained positively charged during the adsorption mechanism.

The ion-exchange mechanism with the bentonite was further considered with regards to the ratio of heavy metal ions (Pb^{2+}) adsorbed onto the adsorbent to the total sum of light metal ions (Ca^{2+}, Mg^{2+}, Na^+, K^+) released during adsorption process. These light metal ions can be typically found as exchangeable cations on bentonites. The mathematical ratio equation (abbreviated as $R_{b/r}$) was given by Sciban et al. (2006), and is presented in Equation 10.

$$R_{b/r} = \frac{[Pb^{2+}]}{[Ca^{2+}]+[Mg^{2+}]+\frac{[Na^{+}]}{2}+\frac{[K^{+}]}{2}+\frac{[H^{+}]}{2}} \quad (10)$$

The concentrations of all cations involved are expressed in mmol/L. The adsorption process is considered predominantly an ion-exchange mechanism with the bentonite when the $R_{b/r}$ value is equal to unity. While a higher $R_{b/r}$ value indicates that the sum of cations released is smaller compared to the amount of Pb(II) ions adsorbed (Sciban et al., 2006; Ngah and Fatinathan, 2009, 2010) and would thus infer Pb(II) ions would be interacting with the chitosan. The calculated $R_{b/r}$ values obtained for adsorption of Pb(II) ions onto Bt-Ch composites and beads are shown in Figure 8. The Rb/r values were determined based on offered Pb(II) levels ranging from 2 to 90 mg/L. Graphs showing the simultaneous adsorption of Pb(II) ions and displacement of Na^{+}, Ca^{2+}, Mg^{2+}, K^{+}, and H^{+} by Bt-Ch composites and beads are presented in in the Supplementary section (Figure S13). The data in Figures 8 and S13 are derived from the same adsorption experiments but are presented differently to allow a different visualisation of the data. Figure S14 presents data from the same experiments but the amounts of Pb(II) offered, Pb(II) adsorbed and Na^{+} released are expressed as relative percentages of the total cation exchange capacity. The data has also considered, the divalent and monovalent nature of Pb and Na, the amounts of clay present in the samples as derived from the TGA data (Figure 1) and ignored the release of the other light metal cations (Ca^{2+}, Mg^{2+}, K^{+}) during the uptake of Pb(II) ions as they are minimal and insignificant.

Taking first the Rb/r values and the composites into consideration there is a trend for the Rb/r values to increase as offered Pb(II) levels increase for the 90%Bt-10%Ch and 70%Bt-30%Ch samples whereas for 50%Bt-50%Ch they remain level with Rb/r values around unity.

Rb/r values below unity, as observed for the composites treated with 10 mg/L, would suggest the release of Na^+ cations present in excess of the cation exchange sites. As the concentration of Pb(II) ions offered increased further the Rb/r values reached unity suggesting more cation exchange with the clay was occurring and with highest Pb(II) ion offered concentrations the data inferred their adsorption on to chitosan became more dominant. When taking into account the amounts of clay present and presenting the data with respect to the CEC (Figure S14) the relative extent of adsorption of Pb(II) onto the chitosan rather than the clay becomes more evident as both the amounts of Pb(II) offered are increased and the amounts of clay in the Bt-Ch samples decreased.

For the beads A and B samples, the Rb/r values are mostly below unity suggesting higher amounts of Na^+ cations being released, this suggests that despite deducting the amounts of Na^+ released in the control experiment (i.e. that released from the Bt-Ch samples in the absence of Pb) even more Na^+ ions are released when exposed to Pb (II), perhaps this is related to Na^+ cations interacting strongly with the chitosan that are not easily washed away, but when in the presence of Pb(II) are released. The higher levels of Na in the beads A and B compared to composites are due to use of NaOH to precipitate the chitosan and form the beads (as evidenced from XRF; Supplementary section, Table S3). Figure S14 demonstrates the higher amounts of Na^+ ions released more clearly because the data points for Na^+ are mostly higher than those for Pb, the values on the axis for amounts of the divalent Pb(II) adsorbed are purposely double to directly compare with the single valent Na^+ ions (since 2 Na^+ cations are exchanged for 1 Pb^{2+} cation). When considering the amounts of Pb adsorbed and Na released with beads A and B, and with respect to the CEC they are more comparable

and suggest more adsorption through a cation exchange mechanism rather with the chitosan.

The levels of Pb(II) offered (10–90 ppm) occur within the steeply increasing region of the adsorption isotherms (Figure 5) and before maximum adsorption occurs so it is interesting to see that for the beads and prior to full monolayer coverage the data suggests the dominant adsorption mechanism is via a cation exchange mechanism despite the adsorption capacities of the beads are significantly enhanced by the presence of the chitosan.

Also interesting is that although the composites contain similar amounts of chitosan after processing, the composite that was initially treated with the least amount of chitosan (90%Bt-10%Ch) experiences a more prevalent cation exchange mechanism despite the XRF data showing the available sodium exchangeable cations are similar for all composites. Perhaps, the additional chitosan which is within the interlayer space (as evidenced by XRD) may inhibit the release of Na(I) from or the passage of Pb(II) to the exchange sites.

To further understand the adsorption process of Pb(II) ions, FTIR spectra were collected for Bt-Ch beads before and after Pb(II) adsorption to identify the possible sites of Pb(II) binding (see Supplementary section; Figures S15, S16 and S17). Unfortunately, no major changes or evidence was observed. Previous study reported that both nitrogen and oxygen atoms (of the amino and hydroxyl groups, respectively) are the main adsorption sites for Pb(II) ions when adsorbed onto chitosan-bentonite composites (Morales Futalan et al., 2010), though the contribution from oxygen atoms seems to be less significant compared to nitrogen atoms (Jin and Bai, 2002). There are lone pairs of electrons on both nitrogen and oxygen atoms which can be complexed with metal ions via electron pair sharing, however due to the stronger attraction of the lone pair of electrons to the nucleus associated with the

oxygen atom compared to that in the nitrogen atom, the tendency to donate the lone pair of electrons for sharing with a metal ion will be greater for nitrogen atoms than with oxygen atoms (Jin and Bai, 2002). The nitrogen groups may therefore contribute majorly to the Pb(II) adsorption process which as described by the Freundlich isotherm fitting is chemical adsorption. Overall, the scheme illustrating the possible adsorption mechanisms concerning the adsorption of Pb(II) ions onto Bt-Ch beads-A is shown in Figure 9.

It is appreciated that the adsorption mechanism is complicated especially since there are different adsorption sites associated with either the chitosan or bentonite. If considering chitosan alone and that at pH 4.5 the amine groups would be protonated it would be unlikely for an electrostatic interaction to occur with the also positively charged Pb^{2+}. This therefore would support the dominant cation exchange mechanism with the bentonite (specifically montmorillonite) suggested above and would be acceptable because the driving force for cation exchange of Pb^{2+} with Na^{+} within the interlayer is the poorer solubility of the $PbNO_3$ in water compared to $NaNO_3$ rather than an electrostatic interaction. To complicate matters further, although there is no evidence here for complexation with chitosan and Pb(II) it could be a possibility. Also adsorption linked to the slightly polar ether and/or hydroxyl groups of chitosan could not be ruled out at this low pH. Furthermore, when chitosan and bentonite are combined in such close proximity, new complexation adsorption sites could be available.

4.0 Conclusion

A bio-hybrid and functional adsorbent based on natural, abundant, low-cost, and environmentally friendly resources was successfully synthesised. A series of bentonite-

chitosan composites (via solution blending method) and beads (via precipitation method) were prepared and characterised by XRF, TGA, XRD and FTIR.

Beads synthesised via the precipitation method exhibited higher yields than composites samples prepared via the solution blending method and was due to chitosan lost during the washing stage. XRF analysis of the composites enabled insight into the quantities of exchangeable sodium cations available for exchange with Pb(II), whilst TGA confirmed the beads contained more chitosan than the composites. XRD show that less chitosan could be intercalated into the interlayers of the bentonite when added to the chitosan solution as a powder (beads B) rather than as an aqueous dispersion (composites and beads A). When intercalated, the interlayer spacings increased from mono-layers to bi-layers structures as chitosan loading increased.

Excellent extents of adsorption were obtained for all the prepared Bt-Ch composites and beads and could match that of the pristine chitosan when mixed in the optimum combination (50%Bt-50%Ch – beads B), the advantage of the combination being a more stable and manageable adsorbent. The experimental adsorption data correlated well with both Langmuir and Freundlich isotherm models and high values for maximum Langmuir monolayer Pb(II) adsorption capacities (Q_{max}) were recorded for all Bt-Ch composites and beads ranging from 42.5 ± 4.2 to 94.6 ± 5.6 mg/g. Generally, with increasing chitosan content the amount of Pb (II) adsorbed increased, though the chitosan distribution within the interlayer space of the bentonite clay also had a pronounced effect on the Pb(II) uptake. Chitosan positioned outside the interlayer with beads B led to higher Pb(II) uptake that was associated with a cation exchange mechanism. Whilst the formation of composites which always resulted in relative low chitosan loadings and located within the interlayer space led

to Pb (II) adsorption associated with the chitosan. For beads A with similar chitosan loadings to beads B, but more located within the interlayer a predominantly cation exchange adsorption mechanism was observed.

When comparing Langmuir monolayer maximum adsorption capacities at relative Bt-Ch loadings, beads-B always provided the highest and 50%Bt-50%Ch-Beads B produced the overall highest (94.6 mg/g) and thus deemed the optimal adsorbent. This was linked to the chitosan being located mostly outside the interlayer space (presumably enhancing more cation exchange with the clay) and the higher chitosan loading. Care should be taken in that some chitosan was washed from the adsorbent during repeated use, although this could be captured and reused if a problem. The 90%Bt-10%Ch-beads B sample which did not lose any chitosan still provided a high maximum adsorption capacity (69.2 mg/g) and this was still higher when compared to the other adsorbents. Variance in maximum adsorption capacities was observed for all adsorbents, but all showed excellent removal efficiencies at a typical Pb concentration (100 mg/L) encountered in contaminated wastewater.

Adsorption of Pb(II) from a competing multi-ion component solution by Bt-Ch composites and beads was significantly affected. The developed Bt-Ch composites and beads exhibited good potential for re-use after many cycles of regeneration up to the fifth cycle. Thus, indicating the potential of using Bt-Ch composites and beads a cost-effective adsorbent for removal of Pb(II) ions from both drinking and wastewater.

Declaration of Competing Interest

The authors declare that they do not have any identified personal or financial conflicts of interest which might have had an impact on the research findings presented in this article.

CRediT authorship contribution statement

Hassan Majiya: Funding acquisition, Conceptualisation, Data curation, Writing- Original draft preparation, Writing- Reviewing and Editing

Francis Clegg: Writing- Reviewing and Editing, Supervision.

Chris Sammon: Supervision.

Acknowledgement

Hassan Majiya is grateful to Sheffield Hallam University, UK, for allowing him to conduct his research work for his PhD at the Materials and Engineering Research Institute (MERI). The project is financially supported by Tertiary Education Trust Fund (TETFund) in Nigeria.

References

Abollino, O., Aceto, M., Malandrino, M., Sarzanini, C., Mentasti, E., 2003. Adsorption of heavy metals on Na-montmorillonite. Effect of pH and organic substances. Water Res. 37, 1619–1627.

Akpomie, K.G., Dawodu, F.A., Adebowale, K.O., 2015. Mechanism on the sorption of heavy metals from binary-solution by a low cost montmorillonite and its desorption potential. Alexandria Eng. J. 54, 757–767.

Alemdar, A., Ece, O.I., Atici, O., 2005. The rheological properties and characterization of bentonite dispersions in the presence of non-ionic polymer PEG. J. Mater. Sci. 40, 171–177.

Babel, S., Agustiono Kurniawan, T., 2003. Low-cost adsorbents for heavy metals uptake from contaminated water: a review, J. Hazard. Mater. 97, 219–243.

Benhouria, A., Islam, M.A., Zaghouane-Boudiaf, H., Boutahala, M., Hameed, B.H., Islam, A., Zaghouane-Boudiaf, H., Boutahala, M., Hameed, B.H., 2015. Calcium alginate–bentonite–activated carbon composite beads as highly effective adsorbent for methylene blue. Chem. Eng. J. 270, 621–630.

Breen, C., Clegg, F., Hughes, T.L., Yarwood, J., 2000. Thermal and spectroscopic characterization of N-methylformamide/Ca-, Mg-, and Na-exchanged montmorillonite intercalates. Langmuir 16, 6648–6656.

Breen, C., Clegg, F., Thompson, S., Jarnstrom, L., Johansson, C., 2019. Exploring the interactions between starches, bentonites and plasticizers in sustainable barrier coatings for paper and board. Appl. Clay Sci. 183, 105272.

Chen, L., Wu, P., Chen, M., Lai, X., Ahmed, Z., Zhu, N., Dang, Z., Bi, Y., Liu, T., 2018. Preparation and characterization of the eco-friendly chitosan/vermiculite biocomposite with excellent removal capacity for cadmium and lead. Appl. Clay Sci. 159, 74–82.

Chen, Y., He, M., Wang, C., Wei, Y., 2014. A novel polyvinyltetrazole-grafted resin with high from aqueous solutions . J. Mater. Chem. A 10444–10453.

Cho, D.W., Jeon, B.H., Chon, C.M., Kim, Y., Schwartz, F.W., Lee, E.S., Song, H., 2012. A novel chitosan/clay/magnetite composite for adsorption of Cu(II) and As(V). Chem. Eng. J. 200–202, 654–662.

Crini, G., 2005. Recent developments in polysaccharide-based materials used as adsorbents in wastewater treatment. Prog. Polym. Sci. 30, 38–70.

Darder, M., Colilla, M., Ruiz-Hitzky, E., 2004. Chitosan-clay nanocomposites: application as electrochemical sensors. Appl. Clay Sci. 28, 199–208.

Darder, M., Colilla, M., Ruiz-Hitzky, E., 2003. Biopolymer-Clay Nanocomposites Based on Chitosan Intercalated in Montmorillonite. Chem. Mater. 15, 3774–3780.

Das, S., Samanta, A., Gangopadhyay, G., Jana, S., 2018. Clay-Based Nanocomposites as Recyclable Adsorbent toward Hg(II) Capture: Experimental and Theoretical Understanding. ACS Omega 3, 6283−6292

Datta, D., Uslu, H., 2017. Adsorptive separation of lead (Pb2+) from aqueous solution using tri-n-octylamine supported montmorillonite. J. Chem. Eng. Data 62, 370–375.

Deng, R., Huang, D., Zeng, G., Wan, J., Xue, W., Wen, X., Liu, X., Chen, S., Li, J., Liu, C., Zhang, Q., 2019. Decontamination of lead and tetracycline from aqueous solution by a promising carbonaceous nanocomposite: Interaction and mechanisms insight. Bioresour. Technol. 283, 277–285.

Fei, Y., Hu, Y.H., 2022. Design, synthesis, and performance of adsorbents for heavy metal removal from wastewater: a review. J. Mater. Chem. A 10, 1047–1085.

Foo, K.Y., Hameed, B.H., 2010. Insights into the modeling of adsorption isotherm systems. Chem. Eng. J. 156, 2–10.

Freundlich, H., 1906. Über die Adsorption in Lösungen. Z Phys. Chem. 57, 385–471.

Giannakas, A. and P.M., 2018. Chitosan/Bentonite Nanocomposites for Wastewater Treatment : A Review. J. Nanochemistry Nanotechnol. 1, 1–17.

Gopal Bhattacharyya, K., Gupta, S. Sen, 2008. Adsorption of a few heavy metals on natural and modified kaolinite and montmorillonite: A review. Adv. Colloid Interface Sci. 140, 114–131.

Guibal, E., 2004. Interactions of metal ions with chitosan-based sorbents: a review. Sep. Purif. Technol. 38, 43–74.

H. L. Giles, P. W. Hurley, H.W.M.W., 1995. Simple approach to the analysis of oxides, silicates and carbonates using x-ray fluorescence spectrometry. X-ray Spectrom. 24, 205–218.

Hall, K.R., Eagleton, L.C., Acrivos, A., Vermeulen, T., 1966. Pore- and solid-diffusion kinetics in fixed-bed adsorption under constant-pattern conditions. Ind. Eng. Chem. Fundam. 5, 212–223.

Hassan, M.M., Nuhu, A.A., Sallau, M.S., Majiya, H.M., Mohammed, A.K., 2015. Zamfara lead poisoning saga: Comparison of lead contamination level of water samples and lead poisoning in Bagega Artisanal gold mining district, Nigeria. J. Chem. Pharm. Res. 7, 7–12.

He, R., Li, W., Deng, D., Chen, W., Li, H., Wei, C., Tang, Y., 2015. Efficient removal of lead from highly acidic wastewater by periodic ion imprinted mesoporous SBA-15 organosilica combining metal coordination and co-condensation. J. Mater. Chem. A 3, 9789–9798.

Hu, C., Zhu, P., Cai, M., Hu, H., Fu, Q., 2017. Comparative adsorption of Pb(II), Cu(II) and Cd(II) on chitosan saturated montmorillonite: Kinetic, thermodynamic and equilibrium studies. Appl. Clay Sci. 143, 320–326.

Jane Calagui, M.C., Senoro, D.B., Kan, C.-C., Salvacion, J.W., Morales Futalan, C., Wan, M.-W., 2014. Adsorption of indium(III) ions from aqueous solution using chitosan-coated bentonite beads. J. Hazard. Mater. 277, 120–126.

Jin, L., Bai, R., 2002. Mechanisms of lead adsorption on chitosan/PVA hydrogel beads. Langmuir 18, 9765–9770.

Kadir, M.F.Z., Aspanut, Z., Majid, S.R., Arof, A.K., 2011. FTIR studies of plasticized poly(vinyl alcohol)-chitosan blend doped with NH_4NO_3 polymer electrolyte membrane. Spectrochim. Acta - Part A Mol. Biomol. Spectrosc. 78, 1068–1074.

Kang, C., Li, W., Tan, L., Li, H., Wei, C., Tang, Y., 2013. Highly ordered metal ion imprinted mesoporous silica particles exhibiting specific recognition and fast adsorption kinetics. J. Mater. Chem. A 1, 7147–7153.

Kotal, M., Bhowmick, A.K., 2015. Polymer nanocomposites from modified clays: Recent advances and challenges. Prog. Polym. Sci. 51, 127–187.

Langmuir, I., 1916. The constitution and fundamental properties of solids and liquids. J. Am. Chem. Soc. 38, 2221–2295.

Lertsutthiwong, P., Noomun, K., Khunthon, S., Limpanart, S., 2012. Influence of chitosan characteristics on the properties of biopolymeric chitosan-montmorillonite. Prog. Nat. Sci. Mater. Int. 22, 502–508.

Lima Patrício, A.C., da Silva, M.M., de Freires Sousa, A.K., Mota, M.F., Freire Rodrigues, M.G., 2012. SEM, XRF, XRD, nitrogen adsorption, foster's swelling and capacity adsorption characterization of cloisite 30 B. Mater. Sci. Forum 727–728.

Liu, Q., Yang, B., Zhang, L., Huang, R., 2015. Adsorption of an anionic azo dye by cross-linked chitosan/bentonite composite. Int. J. Biol. Macromol. 72, 1129–1135.

Liu, J., Zheng, L., Li, Y., Free, M., Yang, M., 2016. Adsorptive recovery of palladium(II) from aqueous solution onto cross-linked chitosan/montmorillonite membrane. RSC Adv. 6, 51757–51767.

Liu, W., Ma, B., Li, F., Fu, Y., Tai, J., Zhou, Y., Lei, L., 2016. Reduction of lead dioxide with oxalic acid to prepare lead oxide as the positive electrode material for lead acid batteries. RSC Adv. 6, 108513–108522.

Lopez-Ramon, M. V, Stoeckli, F., Moreno-Castilla, C., Carrasco-Marin, F., 1999. On the characterization of acidic and basic surface sites on carbons by various techniques. Carbon 37, 1215–122.

Lourdes Dalida, M.P., Francia Mariano, A. V, Futalan, C.M., Kan, C.-C., Tsai, W.-C., Wan, M.-W., 2011. Adsorptive removal of Cu(II) from aqueous solutions using non-crosslinked and crosslinked chitosan-coated bentonite beads. DES 275, 154–159.

Majiya, H., Chowdhury, K.F., Stonehouse, N.J., Millner, P., 2019. TMPyP functionalised chitosan membrane for efficient sunlight driven water disinfection. J. Water Process Eng. 30, 100475.

Majiya, H.M., 2022. Remediation of Heavy Metals from Water using Modified Clay-Chitosan Composites. PhD Thesis, Sheffield Hallam University, 1–333.

Morales Futalan, C., Kan, C.-C., Lourdes Dalida, M., Hsien, K.-J., Pascua, C., Wan, M.-W., 2010. Comparative and competitive adsorption of copper, lead, and nickel using chitosan immobilized on bentonite. Carbohydr. Polym. 83, 528–536.

Moussout, H., Ahlafi, H., Aazza, M., Amechrouq, A., 2018. Bentonite/chitosan nanocomposite: Preparation, characterization and kinetic study of its thermal degradation. Thermochim. Acta 659, 191–202.

Miretzky, P., Cirelli, A.F., 2009. Hg(II) removal from water by chitosan and chitosan

derivatives: A review. J. Hazard. Mater. 167, 10–23.

Muzzarelli, R.A.A., 1977. Chitin. Pergamon Press, Oxford.

Nesic, A.R., Velickovic, S.J., Antonovic, D.G., 2012. Characterization of chitosan/montmorillonite membranes as adsorbents for Bezactiv Orange V-3R dye. J. Hazard. Mater. 209, 256–263.

Ngah, W.S.W., Fatinathan, S., 2010. Pb(II) biosorption using chitosan and chitosan derivatives beads: Equilibrium, ion exchange and mechanism studies. J. Environ. Sci. 338–346.

Ngah, W.S.W., Fatinathan, S., 2009. Adsorption characterization of Pb(II) and Cu(II) ions onto chitosan-tripolyphosphate beads: Kinetic, equilibrium and thermodynamic studies. J. Environ. Manage. 91, 658–969.

Nuhu, A.A., Hassan, M.M., 2014. Heavy Metal Pollution: The Environmental Impact of Artisanal Gold Mining on Bagega Village of Zamfara State, Nigeria. RJPBCS 5, 306–313.

Oladipo, A.A., Gazi, M., 2015. Nickel removal from aqueous solutions by alginate-based composite beads: Central composite design and artificial neural network modeling. J. Water Process Eng. 8, e81–e91.

Oladipo, A.A., Gazi, M., 2014. Enhanced removal of crystal violet by low cost alginate/acid activated bentonite composite beads: Optimization and modelling using non-linear regression technique. J. Water Process Eng. 2, 43–52.

Pandey, S., Mishra, S.B., 2011. Organicâ€“inorganic hybrid of chitosan/organoclay bionanocomposites for hexavalent chromium uptake. J. Colloid Interface Sci. 361, 509–520.

Pereira, F.A.R., Sousa, K.S., Cavalcanti, G.R.S., Fonseca, M.G., de Souza, A.Ô.G., Alves, A.P.M., 2013. Chitosan-montmorillonite biocomposite as an adsorbent for copper (II) cations from aqueous solutions. Int. J. Biol. Macromol. 61, 471–478.

Pillai, C.K.S., Paul, W., Sharma, C.P., 2009. Chitin and chitosan polymers: Chemistry, solubility and fiber formation. Prog. Polym. Sci. 34, 641–678.

Ren, Z., Kong, D., Wang, K., Zhang, W., 2014. Preparation and adsorption characteristics of an imprinted polymer for selective removal of Cr(vi) ions from aqueous solutions. J. Mater. Chem. A 2, 17952–17961.

Rinaudo, M., 2006. Chitin and chitosan: Properties and applications. Prog. Polym. Sci 31, 603–632.

Ruiz-Hitzky, E., Darder, M., Aranda, P., 2005. Functional biopolymer nanocomposites based

on layered solids. J. Mater. Chem. 15, 3650–3662.

Saad, D.M., Cukrowska, E.M., Tutu, H., 2013. Selective removal of mercury from aqueous solutions using thiolated cross-linked polyethylenimine. Appl. Water Sci. 3, 527–534.

Sciban, M., Klašnja, M., Škrbić, B., 2006. Modified softwood sawdust as adsorbent of heavy metal ions from water. J. Hazard. Mater. 136, 266–271.

Shang Tan, W., Su, A., Ting, Y., 2014. Alginate-immobilized bentonite clay: Adsorption efficacy and reusability for Cu(II) removal from aqueous solution. Bioresour. Technol. 160, 115–118.

Taghavi, R., Rostamnia, S., Farajzadeh, M., Karimi-Maleh, H., Wang, J., Kim, D., Jang, H.W., Luque, R., Varma, R.S., Shokouhimehr, M., 2022. Magnetite Metal-Organic Frameworks: Applications in Environmental Remediation of Heavy Metals, Organic Contaminants, and Other Pollutants. Inorg. Chem. 61, 15747–15783.

Tirtom, V.N., Dinçer, A., Becerik, S., Aydemir, T., Çelik, A., 2012a. Removal of lead (II) ions from aqueous solution by using crosslinked chitosan-clay beads. Desalin. Water Treat. 39, 76–82.

Tirtom, V.N., Dinçer, A., Becerik, S., Aydemir, T., Çelik, A., 2012b. Comparative adsorption of Ni(II) and Cd(II) ions on epichlorohydrin crosslinked chitosan-clay composite beads in aqueous solution. Chem. Eng. J. 197, 379–386.

Tirtom, V.N., ße Dinçer, A., Becerik, S., Aydemir, T., Çelik, A., 2012c. Comparative adsorption of Ni(II) and Cd(II) ions on epichlorohydrin crosslinked chitosan-clay composite beads in aqueous solution. Chem. Eng. J. 197, 379–386.

Tran, H.N., You, S.J., Hosseini-Bandegharaei, A., Chao, H.P., 2017. Mistakes and inconsistencies regarding adsorption of contaminants from aqueous solutions: A critical review. Water Res. 120, 88–116.

Vakili, M., Deng, S., Cagnetta, G., Wang, W., Meng, P., Liu, D., Yu, G., 2019. Regeneration of chitosan-based adsorbents used in heavy metal adsorption: A review. Sep. Purif. Technol. 224, 373–387.

Wan, M.-W., Kan, C.-C., Rogel, B.D., Lourdes, M., Dalida, P., 2010. Adsorption of copper (II) and lead (II) ions from aqueous solution on chitosan-coated sand. Carbohydr. Polym. 80, 891–899.

Wan, M.-W., Petrisor, I.G., Lai, H.-T., Kim, D., Fu Yen, T., 2004. Copper adsorption through

chitosan immobilized on sand to demonstrate the feasibility for in situ soil decontamination. Carbohydr. Polym. 55, 249–254.

Wang, H., Tang, H., Liu, Z.Z., Zhang, X., Hao, Z., Liu, Z.Z., 2014. Removal of cobalt(II) ion from aqueous solution by chitosan-montmorillonite. J. Environ. Sci. (China) 26, 1879–1884.

Wang, X., Liu, W., Tian, J., Zhao, Z., Hao, P., Kang, X., Sang, Y., Liu, H., 2014. application in a continuous fi ltering removal device for heavy metal ions †. J. Mater. Chem. A 2599–2608.

Webi, T.W., Ranjit K. Chakravort, 1974. Pore and Solid Diffusion Models for Fixed-Bed Adsorbers. AIChE J. 20, 228–238.

Worch, E., 2012. Adsorption Technology in Water Treatment: Fundamentals, Processes, and Modeling. De Gruyter, Inc., 01062 Dresden Germany.

Yang, S., Zhao, D., Zhang, H., Lu, S., Chen, L., Yu, X., 2010. Impact of environmental conditions on the sorption behavior of Pb(II) in Na-bentonite suspensions. J. Hazard. Mater. 183, 632–640.

Yvonne Ligaya, Santos, C.M., Dalida, L.P., Rodrigues, D.F., 2013. polymer-based graphene oxide nanocomposite. Mater. Chem. A 1, 3789–3796.

Zhang, J., Han, J., Wang, M., Guo, R., 2017. Fe_3O_4/PANI/MnO_2 core–shell hybrids as advanced adsorbents for heavy metal ions. Mater. Chem. A 4058–4066.

Zhang, L., Hu, P., Wang, J., Huang, R., 2016. Adsorption of Amido Black 10B from aqueous solutions onto Zr (IV) surface-immobilized cross-linked chitosan/bentonite composite. Appl. Surf. Sci. 369, 558–566.

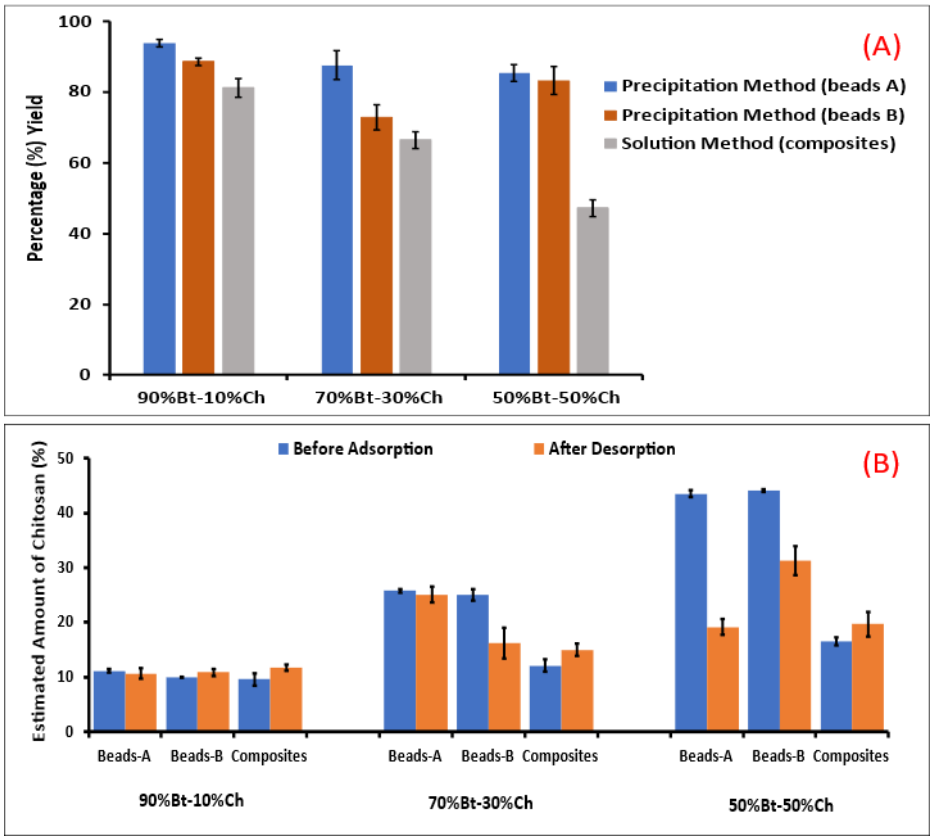

Figure 1 Charts showing A) percentage (%) yield of Bt-Ch composite product recovered via precipitation and solution methods, and B) amounts of chitosan estimated from weight loss values (TGA) of Bt-Ch beads and composites (before adsorption and after 5-cycles of Desorption with dil. HCl). Each bar represents mean ± standard error of three different samples (n = 3). Beads-A = (Bt. suspension + Chitosan solution); beads-B = (powdered Bt. + Chitosan solution).

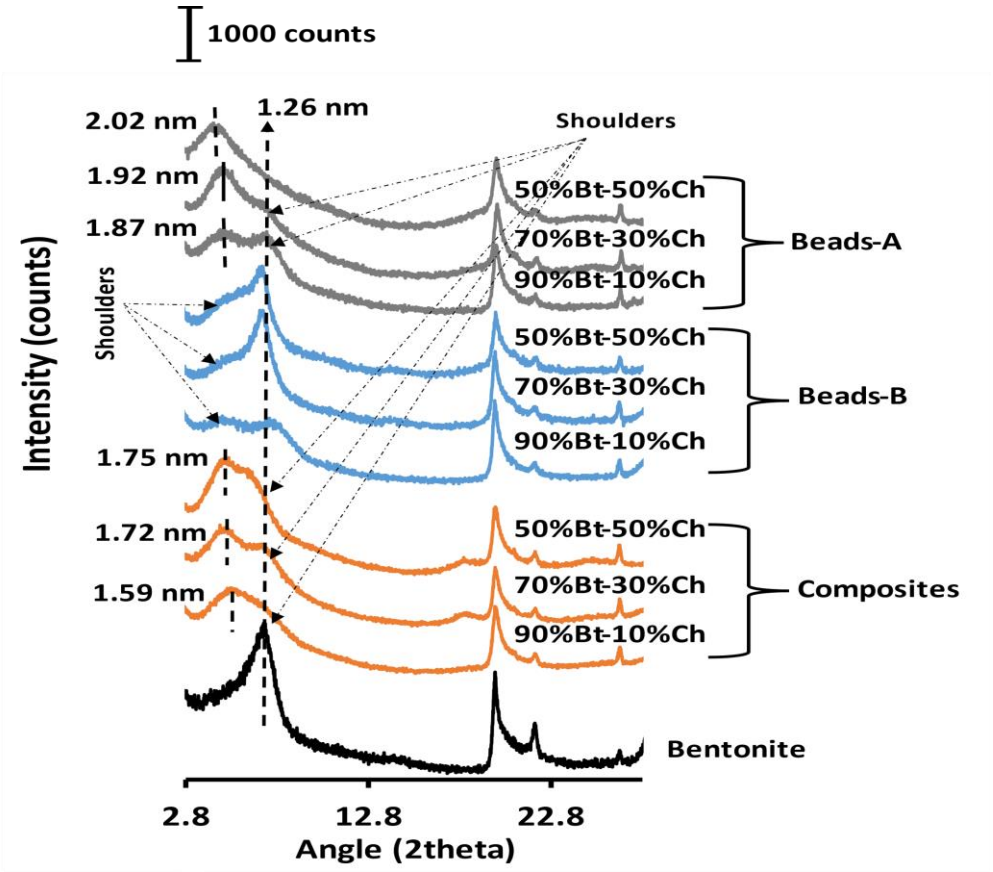

Figure 2 XRD patterns of bentonite, Bt-Ch composites, Bt-Ch beads-B and Bt-Ch beads-A. Note: the diffraction patterns were stacked to make an easy comparison.

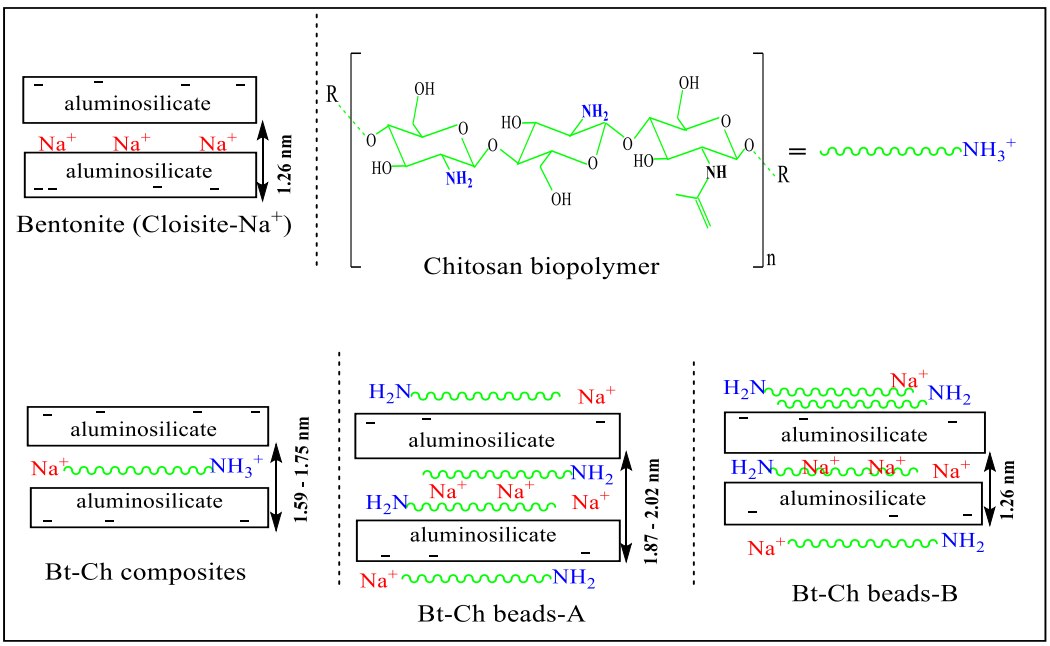

Figure 3 Scheme illustrating how chitosan interacts (or intercalates) with bentonite clay depending on processing method.

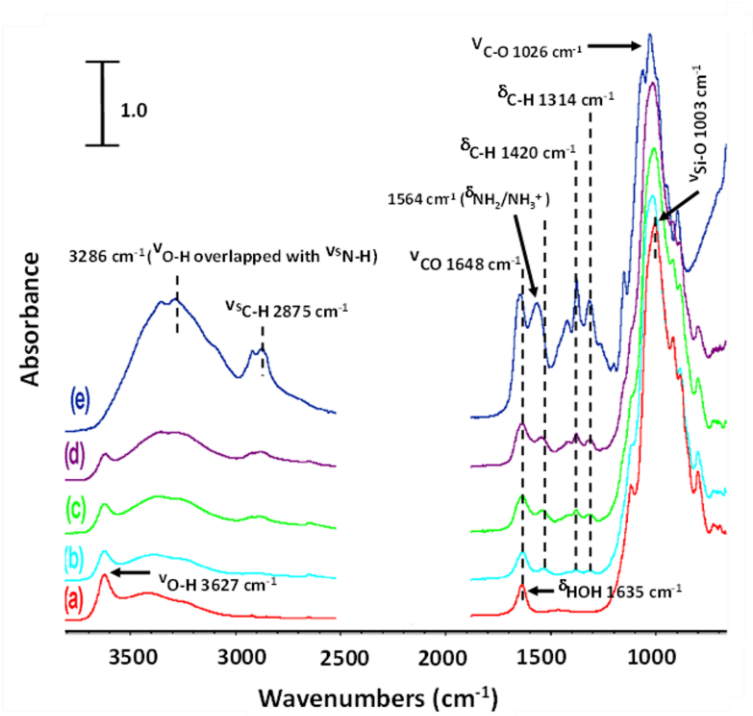

Figure 4 FTIR spectra of (a) pristine bentonite (b) 90%Bt-10%Ch beads-A (c) 70%Bt-30%Ch beads-A (d) 50%Bt-50%Ch beads-A and (e) pure chitosan. V = stretching vibration; δ = bending vibration; v_s = symmetric stretching vibration. Note: the spectra were stacked to make an easy comparison. Spectral region between 1800 – 2500 cm^{-1} is removed due to spectral distortion from diamond crystal of ATR accessory and presence of carbon dioxide.

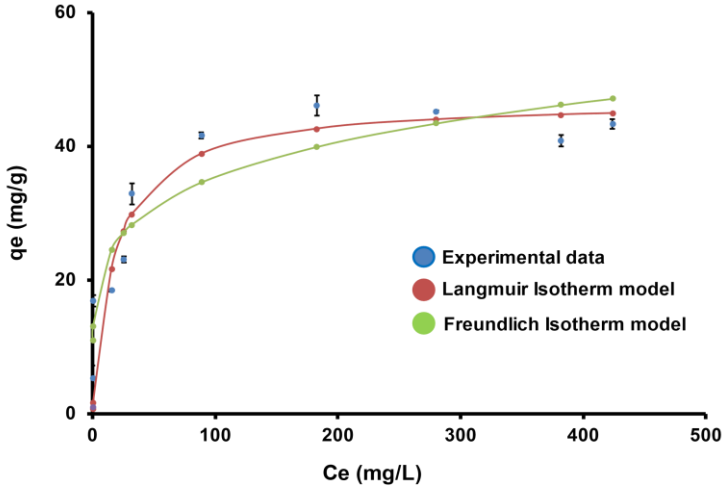

Figure 5 The non-linear Langmuir and Freundlich isotherms for adsorption of Pb (II) by 90%Bt-10%Ch composites. With conditions; pH = 4.5; adsorbent amount = 0.05 g; agitation time (at 230 rpm) = 60 minutes; initial Pb concentrations added to adsorbent = 10-500 mg/L. Each data-point represents mean ± standard deviation of three different experiments (n = 3). Note the data plotted is concentration after equilibrium rather than initial Pb concentrations added to the adsorbents.

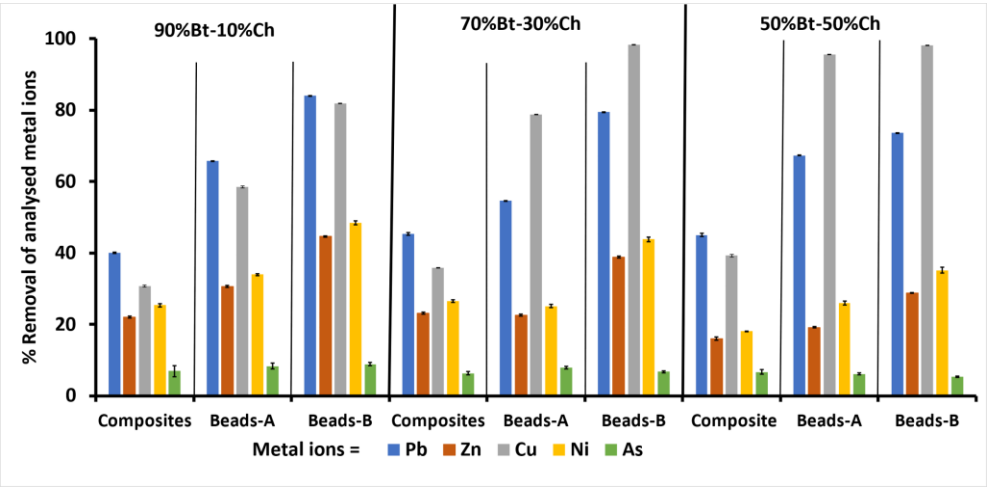

Figure 6 Charts showing the removal efficiencies (%) of various metal ions from multi-component solutions by Bt-Ch composites and beads. Initial concentrations of each metal in multi-component solution = 100 mg/L; pH = 4.5; adsorbent amount = 0.2 g; agitation time (at 230 rpm) = 60 minutes. Each bar represents mean ± standard deviation of three different samples (n = 3).

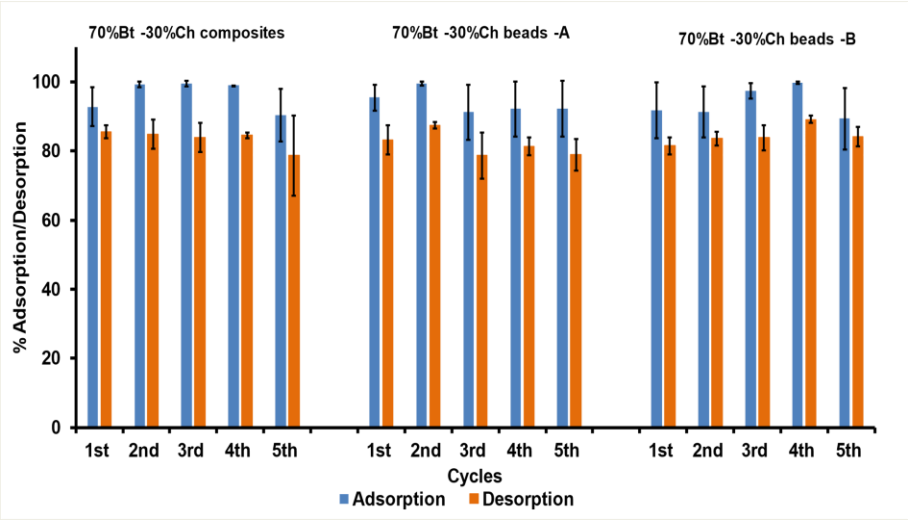

Figure 7 Charts showing the serial % Adsorption/Desorption of Pb(II) ions adsorbed onto 70%Bt-30%Ch composites/beads. Initial Pb concentrations = 150 mg/L; pH = 4.5; adsorbent amount = 0.2 g; adsorption agitation time (at 230 rpm) = 10 minutes; desorbing agent = HCl (1 M); desorption agitation time (at 230 rpm) = 120 minutes. Each bar represents mean ± standard deviation of three (3) different samples (n = 3)

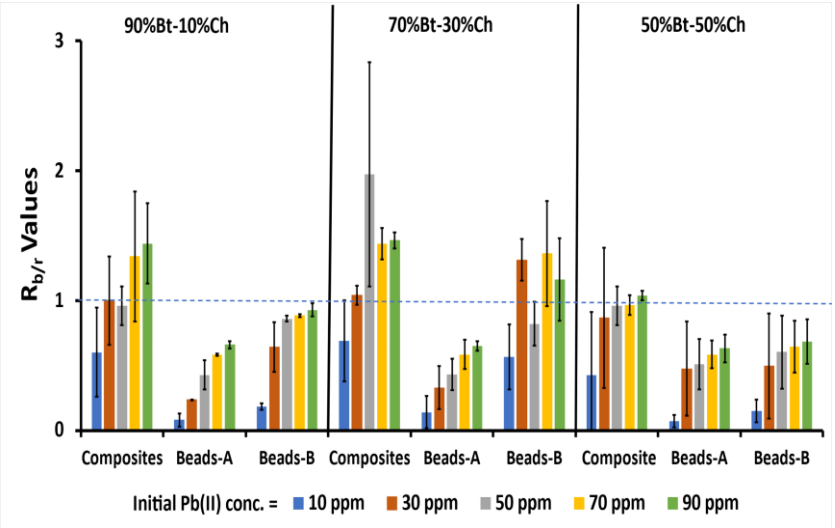

Figure 8 The $R_{b/r}$ values at different Pb (II) concentrations for respective Bt-Ch composites/beads. Note: the dashed blue line denotes the point at which the Rb/r value is equivalent to one (i.e., unity).

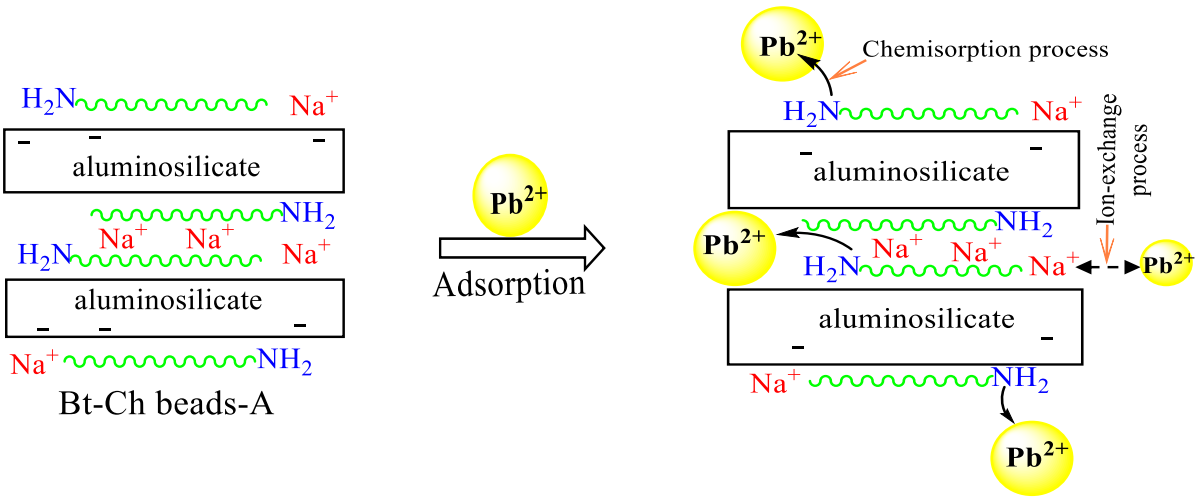

Figure 9 Scheme illustrating possible adsorption mechanisms concerning Pb(II) adsorption onto Bt-Ch beads-A